Fluorescence Fluctuation Spectroscopy in the Presence of Immobile Fluorophores

Joseph P. Skinner, Yan Chen, and Joachim D. Müller
School of Physics and Astronomy, University of Minnesota, Minneapolis, Minnesota 55455

ABSTRACT Fluorescence contributions from immobile sources present a challenge for fluorescence fluctuation spectroscopy (FFS) because the absence of signal fluctuations from stationary fluorophores leads to a biased analysis. This is especially of concern for cellular FFS studies on proteins that interact with immobile structures. Here we present a method that correctly analyzes FFS experiments in the presence of immobile sources by exploiting selective photobleaching of immobile fluorophores. The fluorescence decay due to photobleaching of the immobile species is modeled taking into account the nonuniform illumination volume. The experimentally observed decay curve serves to separate the mobile and immobile fluorescence contribution, which is used to calculate the molecular brightness from the FFS data. We experimentally verify this approach in vitro using the fluorescent protein EGFP as our immobilized species and a diffusing dye of a different color as the mobile one. For this special case, we also use an alternative method of determining the brightness by spectrally resolving the two species. By conducting a dilution study, we show that the correct parameters are obtained using either technique for a wide range of mobile fractions. To demonstrate the application of our technique in living cells, we perform experiments using the histone core protein H2B fused with EGFP expressed in COS-1 cells. We successfully recovered the brightness of the mobile fraction of H2B-EGFP.

INTRODUCTION

Fluorescence fluctuation spectroscopy (FFS) examines kinetic processes and molecular interactions by statistical analysis of equilibrium fluctuations. The technique exploits fluorescence intensity fluctuations of molecules that pass through a very small optical observation volume. A number of analysis tools exist with which to extract information from the intensity fluctuations. The most widely used approach, fluorescence correlation spectroscopy (FCS), is based on the analysis of the correlation function (1). There are many applications for FFS, such as protein diffusion, flow, protein-protein interactions, and protein conformational fluctuations (2,3). Protein oligomerization has been the focus of a number of studies using FFS techniques (4–7). A novel parameter accessible to FFS studies is the molecular brightness, a single molecule parameter that specifies the average photon count rate of a fluorescent molecule (8). Recently, the determination of the brightness using FFS has been shown to be a useful method for quantifying protein interactions and oligomerization in living cells (9–11).

FFS requires that the fluorescent molecules give rise to fluctuations, i.e., by passing through the observation volume. The additional presence of a stationary fluorescence source leads to biases in the analysis of FFS data, because the constant signal adds to the fluorescence intensity without producing fluctuations. Such background fluorescence is typically negligible for most in vitro applications. For cellular systems, the situation is more complicated. Fluorescent proteins that bind to the chromosome or to certain parts of the cytoskeleton may be regarded as immobile over the timescale of a typical experiment. Thus there are many potential cellular applications of FFS where mixtures of mobile and immobile fluorophores are present. We describe here an approach that allows for a quantitative interpretation of FFS experiments in the presence of such mixtures. It is based on the selective photobleaching of immobile fluorophores, which provides a signature for distinguishing signal from mobile and immobile fluorophores. Whereas diffusing molecules are only excited when passing through the two-photon excitation volume, immobile fluorophores located in the two-photon volume are continually excited, resulting in photobleaching even under conditions where bleaching of diffusing molecules is negligible.

Photobleaching of immobile molecules leads to a time-dependent decrease of the fluorescence intensity. Analysis of the fluorescence decay curve distinguishes the intensity contributions from the mobile and immobile fluorophores. This information is used to calculate the brightness and fluctuation amplitude of the FFS data. To experimentally verify the technique, we use the fluorescent protein EGFP because it is widely used for cellular FFS experiments. We first examine the photobleaching kinetics of EGFP while taking the spatial dependence of the excitation volume into account. The technique is applied in vitro using EGFP as the immobilized species and a diffusing dye of a different color as the mobile species. This is a special case in which the mobile and immobile species can be spectrally resolved. Therefore, we describe and apply an independent method to separate the mobile and immobile species using color. The brightness

Submitted June 20, 2007, and accepted for publication November 6, 2007.

Address reprint requests to Joachim D. Müller, University of Minnesota, School of Physics and Astronomy, 116 Church St., SE Minneapolis, MN 55455. Tel: 612-625-4369; Fax: 612-624-4578; E-mail: mueller@physics.umn.edu.

Editor: Enrico Gratton.

0006-3495/08/03/2349/12 $2.00

doi: 10.1529/biophysj.107.115642

values using either technique agree with the calibrated value within experimental error.

The technique has the potential for measuring protein systems interacting with immobile structures in cells. We therefore tested the applicability of our approach by performing this measuring in live COS-1 cells. Our model protein system for these experiments is the chromatin binding histone core protein H2B. This protein has been well studied and is known to show the presence of both mobile and immobile fractions (12–15). We tested our method by measuring mobile fractions of H2B and successfully determined their brightness in living cells.

MATERIAL AND METHODS

Experimental setup

Experiments were conducted on a home-built two-photon fluorescence fluctuation microscope. A mode locked titanium-sapphire laser (Tsunami, Spectra Physics, Mountain View, CA) pumped with an intracavity doubled Nd:YVO_4 (Spectra Physics) laser serves as the excitation source. The beam passes through a beam expander (~5×) before entering a modified Axiovert 200 microscope (Zeiss, Göttingen, Germany) where it is reflected by a dichroic beam splitter (675DCSXR, Chroma Technology, Brattleboro, VT) and focused by a 63× oil immersion objective (NA 1.4) (Zeiss) onto the sample. The emitted fluorescence light is collected by the same objective and separated according to color using a 525 nm dichroic (525DCLPXRU, Chroma Technology) to allow for dual color measurements. Two avalanche photodiode (Model SPCM-AQR-14, PerkinElmer, Vaudreuil, Quebec, Canada) were positioned at the focal point of the tube lens to measure the emitted fluorescence, which is recorded by an FCS data acquisition card (ISS, Champaign, IL) and stored in computer files for further analysis. For single color experiments, the dichroic is removed and all photons are collected by a single avalanche photodiode. Uncorrected emission spectra were taken with a Spectrograph (SpectraPro-2150i, Acton Research, Acton, MA) connected to an imaging charge-coupled device camera (iXon DV887, Andor Technology, South Windsor, CT).

All experiments were conducted with an excitation wavelength of 905 nm. The excitation powers quoted in this article are measured with a power meter (818-F-IR, Newport, Irvine, CA) before the beam enters the objective. For all excitation powers used, photobleaching of the mobile species was negligible. The experiments are performed at excitation powers where the fluorescence intensity of the diffusing species increases quadratically as a function of power. As a further check, the autocorrelation function of the mobile species was measured as a function of power. Experiments were only conducted under conditions where the measured diffusion time was independent of power.

Sample preparation and experimental procedures

The bleaching kinetics of the fluorescence for EGFP was measured by immobilizing His-tagged EGFP on the functionalized surface of glass coverslips (MicroSurfaces, Minneapolis, MN). The functionalized coverslip was mounted on a microscope slide with double stick tape to create a flow cell (~80 μL volume). A 1 mM solution of EGFP was incubated in the flow cell for 10 min before being washed three times with 200 μL of wash buffer (phosphate-buffered saline, 0.5% Triton-X, 20 mM imidazole).

The surface was exposed to excitation light as illustrated by the inset in Fig. 2, and the decay of the fluorescence was recorded. Experiments were conducted by either focusing the beam of the titanium-sapphire laser on the surface, or by exposing a small area of the surface to a uniform beam with an epifluorescence lamp. The kinetic parameters describing the decay curves were determined by fits to models described in the Theory section.

Next, FFS experiments were performed with immobilized EGFP in the presence of a mobile species. The amount of mobile species present was systematically varied by filling the flow cell with different concentrations of the red dye sulforhodamine 101 (SR101, Molecular Probes, Eugene, OR). The 525 nm dichroic was used to separate the emission of SR101 and EGFP into two detection channels. During each measurement, some of the immobilized EGFP is bleached. To start each experiment with unbleached EGFP, the slide containing the immobilized EGFP was moved to a new location between measurements.

The concentration of the stock solution of SR101 was determined by absorption spectroscopy using the extinction coefficient quoted by the manufacturer. SR101 was diluted to nanomolar concentrations in buffer solution (phosphate-buffered saline, 0.5% Trixon-X). His-tagged EGFP protein was purified according to Patterson et al. (16) and diluted in phosphate buffer (Dulbecco's Phosphate Buffered Saline, Cambrex, Walkersville, MA).

COS-1 cells were transiently transfected with H2B-EGFP or cotransfected with H2B-EGFP and EGFP at a 1:1 DNA ratio. All measurements were conducted in the cell nucleus. Highly overexpressed cells and those with abnormal morphology were not measured. To determine the distribution of H2B-EGFP in the nucleus along the axial direction, a piezo-driven z stage (MS-2000XYZ, ASI, Eugene, OR) scanned the focal position of the beam at a very low excitation power across the cell. The position of the focal volume is monitored by the stage controller with submicron resolution. The fluorescence intensity is recorded as a function of depth within the cell.

Data analysis

Routines for calculating the brightness, fitting the fluorescence intensity decay curves, and correcting the brightness were written in IDL (Research Systems, Boulder, CO). We briefly outline the calculation of the decay curves and their analysis. FFS data were sampled at 50 kHz and the resulting photon count sequence was divided into segments of 10,000 data points (0.2 s). To generate the intensity trace, the average of each segment was calculated. The trace was fit to models using experimental uncertainty defined in one of two ways: 1), the standard deviation across multiple identical measurements was calculated, or 2), each 0.2 s interval was approximated as stationary, and the uncertainty was estimated by $\sqrt{\langle k\rangle}/\sqrt{N}$, where $\langle k\rangle$ is the average photon count of the segment and N is the number of data points in the segment. Both methods yielded similar fitting results and residuals as reported in the Results section below. For the second case, it is important to include a correlation term for the diffusing molecules when calculating the error (17). Calculation of the brightness was done using larger segments of the data to improve the signal/noise ratio.

The brightness was determined using the generalized Q-parameter Q_τ instead of the Q-parameter, because of its better signal/noise and robustness with respect to afterpulsing and detector dead time (18),

$$\lambda^* = \frac{Q_\tau^*}{\gamma_2 f_{T_s}(\tau)}, \tag{1}$$

where $f_{T_s}(\tau)$ is a correction factor accounting for the sampling time (18). Equation 1 was evaluated for $\tau = T_s$, where $T_s = 20\ \mu$s is the sampling time at which the data were taken. The corrected brightness λ is determined using Eq. 7. The error quoted for the brightness is the standard deviation calculated using all of the values obtained from the segmented data.

THEORY

We first introduce brightness and its determination from FFS data. Next, we consider the presence of an immobile species and its bias on brightness analysis. Photobleaching of the

immobile species is another complicating factor and will be incorporated into the analysis model.

Brightness

An FFS measurement determines the photon counts $k(t)$ as a function of time with the temporal resolution set by the sampling time T. We consider in the following the short sampling time limit ($T \ll \tau_D$), where the sampling time T is much faster than the diffusion time τ_D, which characterizes the average time for the fluorophore to diffuse across the observation volume. In the short sampling time limit, data are sampled fast enough that the photon count fluctuations track the fluorescence intensity fluctuations due to diffusion of the fluorophore. This leads to simple relationships between the photon count moments and the fluorescence intensity moments (19,20). For example, the average photon counts received per sampling time is the product of the fluorescence intensity $\langle F\rangle$ in units of counts per second and the sampling time, $\langle k\rangle = \langle F\rangle T$.

The brightness λ of a fluorophore characterizes the fluorescence intensity of a single fluorophore. The fluorescence intensity $\langle F\rangle = \lambda N$ of a fluorophore solution is the product of the average number of molecules N in the excitation volume and the brightness of the fluorophore. The average number of photon counts $\langle k\rangle$ is similarly given by

$$\langle k\rangle = \varepsilon N, \tag{2}$$

where ε denotes the average number of photon counts detected from a single fluorophore per sampling time T, and is related to λ via

$$\varepsilon = \lambda T. \tag{3}$$

Both, ε and λ are measures of the brightness of a molecule. We will mainly use λ, because it is independent of the sampling time. The value of the brightness depends on the fluorophore, the excitation power, and other instrumental parameters. However, if instrumental parameters are kept constant, then brightness depends only on the fluorophore species. Brightness has been used to determine the stoichiometry of protein complexes in cells (9). For example, the dimer of two fluorescently tagged proteins carries two fluorophores and has twice the brightness of the monomer.

There are several methods that determine the brightness from experimental data. Here we use moment analysis and extract the brightness from Mandel's Q-parameter,

$$Q = \gamma_2(\lambda T) = \frac{\langle \Delta k^2\rangle - \langle k\rangle}{\langle k\rangle}, \tag{4}$$

with the shape factor γ_2 of the point spread function (PSF) (21).

Immobilization

The above treatment assumes that a single species with brightness λ contributes to the fluorescence signal. The Q-parameter for a mixture of i fluorescent species is determined by the Q-parameter Q_i of the ith species and its average photon count $\langle k_i\rangle$:

$$Q = \sum_i \frac{\langle k_i\rangle}{\langle k_T\rangle} Q_i, \tag{5}$$

where $\langle k_T\rangle = \sum_i \langle k_i\rangle$ is the total average photon count of the sample. We now consider the special case of a mobile and an immobile species, which are denoted by the subscript M and I, respectively. The mobile species introduces fluorescence intensity fluctuations as molecules diffuse in and out of the observation volume. In contrast, the immobile component does not produce fluorescence fluctuations, because the molecules are fixed in space. The distribution of photon counts due to the immobile species is Poissonian, which dictates that the Q-parameter of the immobile species is zero, $Q_I = 0$. The experimental Q-parameter Q^* of the mixture

$$Q^* = \frac{\langle k_M\rangle}{\langle k_T\rangle} Q_M \tag{6}$$

is proportional to the Q-parameter Q_M of the mobile component. If we assume that the mobile species has brightness λ and an average of N molecules in the observation volume, its Q-parameter is $Q_M = \gamma_2 \lambda T$. The apparent brightness λ^* of the mixture of a mobile and immobile species is deduced from its Q-parameter, $Q^* = \gamma_2 \lambda^* T$, which leads to

$$\lambda^* = \lambda f_M, \tag{7}$$

where we introduced the fractional intensity of the mobile species,

$$f_M = \frac{\langle k_M\rangle}{\langle k_T\rangle}. \tag{8}$$

For comparison, the fluctuation amplitude $g(0)$ of a mixture of species is $g(0) = \sum_i g_i(0)(\langle k_i\rangle/\langle k_T\rangle)^2$(18). Thus, for a mobile and immobile species, the fluctuation amplitude is given by

$$g^*(0) = g_M(0) f_M^2. \tag{9}$$

Because the fluctuation amplitude of the mobile species is $g_M(0) = \gamma_2/N$, the apparent number of molecules N^* given by the experimentally accessible fluctuation amplitude $g^*(0) = \gamma_2/N^*$ is related to the actual number of freely diffusing fluorophores by

$$N^* = N\frac{1}{f_M^2}. \tag{10}$$

The presence of an immobile species diminishes both the fluctuation amplitude and the Q-parameter (Eqs. 6 and 9). As a consequence, the experiment reports a biased brightness λ^* and an average number of molecules N^*. If the fractional intensity f_M of the mobile species is known, it is possible to correct the biased parameters according to Eqs. 7 and 10. In principle, the first three moments of the photon counts

determine the fractional intensity f_M (22). However, photobleaching of the immobile species, dead time, and the limited signal/noise render this approach impractical for cellular applications.

Photobleaching

We consider experimental conditions where photobleaching of the mobile fluorophores is negligible. Under such conditions, the fluorescence intensity of the mobile component is constant, $\langle k_M \rangle = \langle F_M \rangle T$. In contrast to diffusing molecules, which are only exposed to the laser beam while passing through the illuminated volume, the immobile molecules located within the excitation volume are exposed to the laser beam during the entire duration of the experiment. As a consequence. photobleaching of the immobile species occurs and leads to a decay of the fluorescence intensity, $\langle k_I(t) \rangle = \langle F_I(t) \rangle T$. The total fluorescence signal $\langle k_T(t) \rangle$ is the sum of the constant signal from the mobile species and the time-dependent signal from the immobile component,

$$\langle k_T(t) \rangle = \langle k_M \rangle + \langle k_I(t) \rangle. \tag{11}$$

The average fluorescence signal depends on time and is therefore nonstationary. Because FFS analysis requires a stationary signal, the brightness cannot be calculated for the whole data set. Instead, we divide the data set into short segments, so that the fluorescence intensity is approximately constant over the time interval t_S of the segment. We calculate the Q-parameter for each data segment according to Eq. 4 to determine $Q^*(t)$. The time-independent brightness of the mobile fraction is expressed with the help of Eq. 7:

$$\lambda = \frac{Q^*(t)}{\gamma_2 f_M(t)}. \tag{12}$$

Next we consider the fluorescence intensity decay of the immobile fraction. For a mixture of species, the average fluorescence intensity at position $\mathbf{r}$ is

$$\langle F_I(\mathbf{r},t) \rangle = \langle k_I(\mathbf{r},t) \rangle / T = \sum_i \lambda_i \, \mathrm{PSF}(\mathbf{r}) c_i(\mathbf{r},t), \tag{13}$$

where the ith species has brightness λ_i and concentration $c_i(\mathbf{r},t)$. The shape of the PSF is given by $\mathrm{PSF}(\mathbf{r})$ with $\mathrm{PSF}(0) = 1$. The total fluorescence is obtained by integrating over space,

$$\langle F_I(t) \rangle = \langle k_I(t) \rangle / T = \sum_i \lambda_i \int \mathrm{PSF}(\mathbf{r}) c_i(\mathbf{r},t) d\mathbf{r}. \tag{14}$$

If the concentration of each species is spatially uniform, $c_i(\mathbf{r},t) = c_{i0}(t)$, then Eq. 14 simplifies to

$$\langle F_I(t) \rangle = \langle k_I(t) \rangle / T = \sum_i \lambda_i V_{PSF} c_{i0}(t) = \sum_i \lambda_i N_i(t) \tag{15}$$

with the volume of the PSF defined as $V_{PSF} = \int \mathrm{PSF}(\mathbf{r}) d\mathbf{r}$ and the number of molecules in the observation volume defined by $N = V_{PSF} c$, where c is expressed in number of molecules per volume.

Fluorescence intensity decay curves I

In the simplest bleaching model, the fluorescent state A with brightness λ converts directly into the nonfluorescent state D, $A \xrightarrow{k_A} D$, where k_A is the rate coefficient of bleaching and depends on the fluorophore, the laser wavelength, and excitation intensity. Because the excitation intensity of the focused laser beam varies across space, the bleach coefficient k_A depends on space (14,23),

$$k_A(\mathbf{r}) = \xi P^n \mathrm{PSF}(\mathbf{r}) = k_{A0} \mathrm{PSF}(\mathbf{r}), \tag{16}$$

where ξ is a constant, P is the laser power, $k_{A0} = \xi P^n$, and n is the number of photons absorbed in the excitation process. The time-dependent concentration of fluorophores in state A is given by

$$c_A(\mathbf{r},t) = c_A(\mathbf{r},0) e^{-k_A(\mathbf{r})t} = c_A(\mathbf{r},0) e^{-k_{A0}\mathrm{PSF}(\mathbf{r})t}. \tag{17}$$

It was assumed that the immobilized fluorophores are uniformly distributed $c_A(\mathbf{r},0) = c_0$. Therefore, $N_0 = c_0 V_{PSF}$ and the time-dependent fluorescence intensity of the immobile component is

$$\langle F_I(t) \rangle = \langle F_I(0) \rangle \int \frac{\mathrm{PSF}(\mathbf{r})}{V_{PSF}} e^{-k_{A0}\mathrm{PSF}(\mathbf{r})t} d\mathbf{r} \tag{18}$$

with $\langle F_I(0) \rangle = \lambda N_0$. In the following, we will use the decay time $\tau = 1/k_{A0}$ instead of the rate coefficient. We introduce the normalized decay function $\phi(\tau,t)$ to write Eq. 18 in compact form:

$$\phi(\tau,t) = \frac{\langle F_I(t) \rangle}{\langle F_I(0) \rangle} = \frac{\langle k_I(t) \rangle}{\langle k_I(0) \rangle} = \int \frac{\mathrm{PSF}(\mathbf{r})}{V_{PSF}} e^{-\mathrm{PSF}(\mathbf{r})t/\tau} d\mathbf{r}. \tag{19}$$

The normalized decay function depends on the explicit shape of the PSF and on the sample geometry. We discuss in the following the decay function for a few cases of interest. The decay function of each model is distinguished by its subscript. Note that the normalized decay function uses the characteristic decay time τ instead of the decay rate coefficient. This notation will be used throughout the manuscript.

For a uniform illumination profile ($\mathrm{PSF}(\mathbf{r}) =$ constant, subscript U) the average photon count is

$$\phi_U(\tau,t) = e^{-t/\tau}. \tag{20}$$

For a two-dimensional system, we approximate the PSF shape by a two-dimensional Gaussian (2DG)

$$\mathrm{PSF}_{2DG}(\rho) = \exp\left(-\frac{2n\rho^2}{w_0^2}\right), \tag{21}$$

where w_0 is the radial beam waist of the beam, ρ is the radial coordinate, and n denotes the number of photons absorbed in the excitation process. The normalized decay function in this case is given by

$$\phi_{2DG}(\tau,t)=\frac{1-\exp(-t/\tau)}{t/\tau}. \quad (22)$$

We will model the decay in three dimensions using a squared Gaussian-Lorentzian PSF for two-photon excitation. The squared Gaussian-Lorentzian (GL) PSF is defined in cylindrical coordinates as

$$\mathrm{PSF}_{GL}(\rho,z)=\frac{w_0^4}{w^4(z)}\exp\left(-\frac{4\rho^2}{w^2(z)}\right) \quad (23)$$

with $w^2(z)=w_0^2(1+z^2/z_r^2)$, and z_r denotes the axial beam waist. Evaluation of Eq. 18 with Eq. 23 leads to the following function for the decay of the average photon counts:

$$\phi_{GL}(\tau,t)={}_2F_2\left(\frac{1}{4},\frac{3}{4};\frac{1}{2},2;-\frac{t}{\tau}\right), \quad (24)$$

with the generalized hypergeometric function ${}_2F_2(a_1,a_2;b_1,b_2;z)$. The definition and properties of the generalized hypergeometric function are described in the literature (24).

Although Eq. 24 describes the decay for an infinite sample in the axial direction, one is more likely to encounter a slab of finite thickness z_{th} in actual experiments. To obtain the decay function when focusing into the center of the slab, one must limit the integration along the axial direction,

$$\phi(\tau,t)=\frac{\langle k_I(t)\rangle}{\langle k_I(0)\rangle}=\frac{t}{\tau}\int_{-z_{th}/2}^{z_{th}/2}\frac{w^2(z)}{V_{PSF}}\left(1-\exp\left[-\frac{w_0^4 t}{w^4(z)\tau}\right]\right)dz. \quad (25)$$

Fig. 1 compares the decay of fluorescence for each of the three models to illustrate the effect of the PSF shape on the bleaching curves. Each normalized decay curve $\phi(\tau,t)$ shown in the figure has a decay time τ equal to 20 s. Adding the spatial dependence of the bleach intensity to the model increases the time it takes for the fluorescence intensity to fully decay. The uniform excitation profile shows the fastest decay, followed by that of the 2DG profile, whereas the GL profile exhibits the slowest decay.

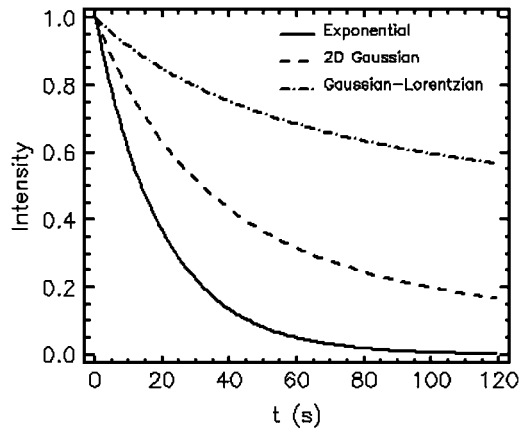

FIGURE 1 Normalized decay curves for three different illumination profiles. The exponential function (*solid line*) corresponds to spatially uniform illumination. The other two decay curves represent two-dimensional Gaussian and Gaussian-Lorentzian illumination profiles. A decay time $\tau = 20$ s was used for all three models.

Fluorescence intensity decay curves II

We previously discussed the most elementary bleaching model. However, to describe our experimental data, we need to consider a more complex model. Consider the two-step model, $A \overset{k_A}{\rightarrow} B \overset{k_B}{\rightarrow} D$, where molecules in the fluorescent state A with brightness $\lambda_A=\lambda$ convert into a fluorescent state B with brightness $\lambda_B=r\lambda$, before reaching the nonfluorescent bleached state D. The brightness ratio of state B to state A is given by the factor r. The transition from A to B is characterized by the rate coefficient k_A, and the corresponding rate coefficient for the transition form B to D is k_B. If we assume initial conditions where all molecules start out in state A and are uniformly distributed, $c_A(\mathbf{r},0)=c_0$ and $c_B(\mathbf{r},0)=0$, the time-dependent concentrations are

$$\begin{aligned}c_A(\mathbf{r},t)&=c_0e^{-k_A(\mathbf{r})t}=c_0e^{-k_{A0}\mathrm{PSF}(\mathbf{r})t}\\ c_B(\mathbf{r},t)&=c_0\frac{k_A(\mathbf{r})}{k_A(\mathbf{r})-k_B(\mathbf{r})}(e^{-k_B(\mathbf{r})t}-e^{-k_A(\mathbf{r})t})\\ &=c_0\frac{k_{A0}}{k_{A0}-k_{B0}}(e^{-k_{B0}\mathrm{PSF}(\mathbf{r})t}-e^{-k_{A0}\mathrm{PSF}(\mathbf{r})t}),\end{aligned} \quad (26)$$

where we used the fact that both rate coefficients depend on the position according to Eq. 16. The normalized decay function $\phi'(\tau_A,\tau_B,t)$ for the two-step bleaching model is derived from Eq. 26 with the help of Eqs. 14 and 19,

$$\phi'(\tau_A,\tau_B,t)=\frac{\langle k_I(t)\rangle}{\langle k_I(0)\rangle}=(1-\alpha)\phi(t,\tau_A)+\alpha\,\phi(t,\tau_B), \quad (27)$$

with $\tau_A=1/k_{A0}$, $\tau_B=1/k_{B0}$, and the amplitude α defined as

$$\alpha=\frac{r}{(1-\tau_A/\tau_B)}. \quad (28)$$

The fluorescence intensity decay for the two-state bleaching system is modeled by inserting the $\phi(\tau,t)$ function corresponding to the PSF of the experimental system into Eq. 27. The time-dependent average photon count signal in the presence of a mobile and immobile species is then described by

$$\langle k_T(t)\rangle=\langle k_M\rangle+\langle k_I(0)\rangle\,\phi'(\tau_A,\tau_B,t). \quad (29)$$

A fit of the experimental curve $\langle k_T(t)\rangle$ to Eq. 29 determines the characteristic decay times (τ_A and τ_B) and the constant offset $\langle k_M\rangle$, which describes the average photon count signal of the mobile fraction. Note that according to Eq. 16, the ratio τ_A/τ_B is independent of the excitation power. By rewriting the fractional intensity of the mobile species using Eq. 29, we get

$$f_M(t) = \frac{\langle k_M \rangle}{\langle k_M \rangle + (\langle k_M \rangle - \langle k_T(0) \rangle)\phi'(\tau_A, \tau_B, t)}. \quad (30)$$

With the help of this equation, we correct the biased brightness λ^* to recover the true brightness λ of the mobile fraction with Eq. 7.

Bleaching and dual-color detection

Consider a system containing two independent species; one immobile and one mobile, where each species is labeled with a different fluorophore. This is a special case where dual-color detection provides an alternative method to calculate the intensity fraction f_M of the mobile species. A dichroic beam splitter spectrally resolves the fluorescence into two separate channels. Ideally the fluorescence from each species would be separated into distinct channels. However, the spectral overlap of the fluorescence leads to cross talk between the detection channels. This spectral cross talk is experimentally characterized by measuring the intensity ratio between the two channels for a given fluorophore. We label the first channel as red (subscript r) and the second as green (subscript g). The cross talk ratio for each species is defined as $x_j = \langle F_{j,r} \rangle / \langle F_{j,g} \rangle$, where $\langle F_{j,i} \rangle$ is the fluorescence intensity of the jth species in the ith channel. Another experimental measure is the total fluorescence intensity $\langle F_{T,i}(t) \rangle$ of each channel and is given by

$$\langle F_{T,i}(t) \rangle = \langle F_{M,i} \rangle + \langle F_{I,i}(t) \rangle, \quad (31)$$

where $\langle F_{M,i} \rangle$ is the intensity of the mobile fraction and $\langle F_{I,i}(t) \rangle$ is the intensity of the immobile fraction in the ith channel. The total fluorescence intensities and the cross talk ratio of the mobile and immobile species (x_M and x_I) allow for the calculation of the fluorescence intensity of each individual species in a channel. For example, the fluorescence intensity $\langle F_{M,r} \rangle$ of the mobile species in the red channel is determined by

$$\langle F_{M,r} \rangle = \frac{x_M}{x_M - x_I}(\langle F_{T,r}(t) \rangle - \langle F_{T,g}(t) \rangle x_I), \quad (32)$$

and the time-dependent intensity ratio of the mobile fraction in the red channel is

$$f_{M,r}(t) = \langle F_{M,r} \rangle / \langle F_{T,r}(t) \rangle. \quad (33)$$

We will later use this method as a control to validate the determination of the mobile intensity fraction from the photobleaching kinetics based on Eq. 30.

RESULTS

Modeling of photobleaching decay curves for immobile EGFP

Because photobleaching will be important in the subsequent measurements, we first establish rate parameters for the fluorescence decay in the absence of a mobile species. For these experiments, purified EGFP was immobilized on a cover slide by its His tag. The surface was then exposed to either focused or spatially uniform light (see *inset* diagram of Fig. 2) and the time-dependent fluorescence was recorded. Photobleaching experiments were first conducted using one-photon, uniform wide-field illumination to eliminate the spatial intensity dependence of the bleaching rate, which would complicate the analysis. The fluorescence decay curve from this experiment is shown in Fig. 2. A single-step bleaching process leads to a monoexponential decay for a uniform illumination profile (Eq. 20), but an attempted fit to a single exponential decay does not describe this data and gives a reduced χ^2 of 13.2 (data not shown). We found that a biexponential model as described by Eqs. 20 and 27 fits the data, giving a reduced χ^2 of 0.5. The returned rate values were $\tau_1 = 117 \pm 5$ s and $\tau_2 = 370 \pm 60$ s with $\alpha = 0.21 \pm 0.05$. This result is consistent with previous photobleaching studies of EGFP (16,25).

Next we turn to two-photon bleaching at 905 nm of immobilized EGFP by focusing laser light onto the surface of the slide. Five decay curves were measured for 2 min at a time and analyzed taking the two-dimensional Gaussian distribution of the excitation intensity into account. Just as is the case for one-photon bleaching, a single rate process is insufficient to describe the kinetics. We therefore modeled the two-photon decay curve using the two-step bleaching model as suggested by the one-photon data. The standard deviation across all five curves was calculated and used as the error in fitting the individual decay curves to Eq. 27 with Eq. 22. A fit to such a curve is shown in Fig. 3 along with the residuals, which describes the data within experimental uncertainty (reduced χ^2 of 0.3). The intensity decay time parameters determined from the average of all five measurements were

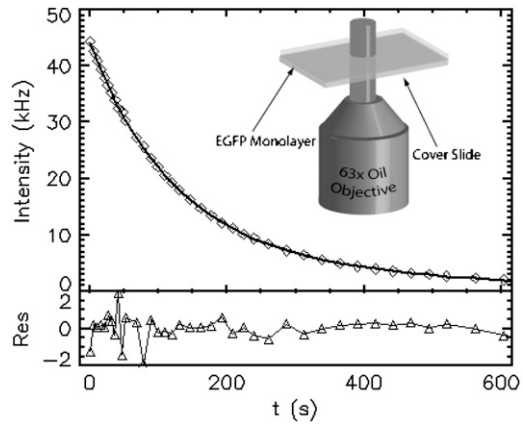

FIGURE 2 One-photon photobleaching of EGFP with spatially uniform illumination. The fluorescence signal of EGFP immobilized on a glass surface (*inset diagram*) is measured. The fit (*solid line*) of the decay curve (*diamonds*) to a sequential two-state model yielded $\tau_1 = 117 \pm 4$ s, $\tau_2 = 370 \pm 60$ s, and $\alpha = 0.21 \pm 0.05$. The normalized residuals of the fit are shown in the lower panel.

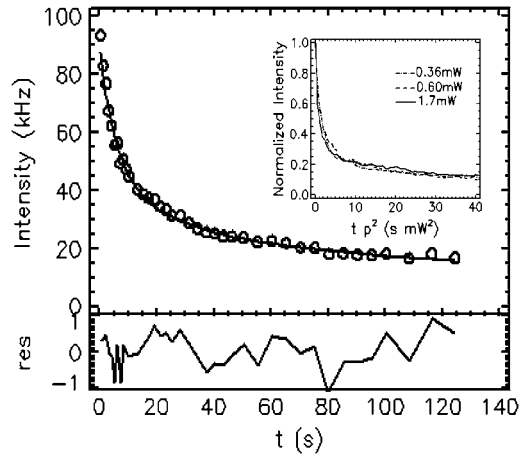

FIGURE 3 Two-photon photobleaching of EGFP immobilized to the surface of a coverslip. The decay curve (*circles*) is fit to a sequential two-state model with a two-dimensional Gaussian illumination profile. The parameters of the fit (*solid line*) are $\tau_1 = 2.9 \pm 1.3$ s, $\tau_2 = 100 \pm 30$, s and $\alpha = 0.26 \pm 0.06$. The normalized residuals of the fit are shown in the lower panel. The inset shows three measurements taken at different powers graphed as a function of time multiplied by the power squared.

$\tau_1 = 2.9 \pm 1.3$ s and $\tau_2 = 100 \pm 30$ s with $\alpha = 0.26 \pm 0.06$. These results will be used below to determine the mobile fraction of a freely diffusing dye added to the sample.

We also checked whether the decay curve obeys the quadratic power dependence indicative of a two-photon process. After defining the normalized time as the product of time and power squared, we examined the power dependence. For quadratic power dependence, the graph of the decay curves as a function of normalized time is independent of power. We measured decay curves for excitation powers ranging from ~0.3 mW to 2 mW and plotted the curves as a function of normalized time (*inset* of Fig. 3). All curves overlap with one another as expected for a two-photon process. Thus, changing the excitation power leads to quadratic changes in the values of τ_1 and τ_2, but their ratio τ_1/τ_2 and α are power independent. This result will be used in the analysis of all subsequent experiments.

Brightness of mobile species

Finding the brightness of a diffusing species in the presence of an immobile component relies on the determination of $f_M(t)$. We outlined two procedures for arriving at the fractional intensity of the diffusing species. The first one depends on photobleaching, whereas the second one relies on a color difference between the mobile and immobile species. To evaluate their performance, we conduct a control experiment where each of the two methods is applied independently and their results are compared. For this experiment, we add a solution of the red dye SR101 to the surface-immobilized EGFP. A 525 nm dichroic mirror in the collection path splits the fluorescence of both dyes into a red and a green channel (*inset* of Fig. 4 *A*). The cross talk ratio of EGFP $x_I = 0.5$ and of SR101 $x_M = 18$ were determined separately. Fig. 4 *A* depicts the measured fluorescence intensity of each channel as a function of time. Because the fluorescence of the green channel $F_{T,g}(t)$ (*dashed line*) contains almost no signal from the red dye as can be seen from the spectral distribution shown in the inset of Fig. 4 *A*, our analysis will focus on the red channel (*solid line*).

We determined the intensity of the mobile fraction in the red channel with each of the two methods. First, we separated the intensity from each species based on color. With Eq. 32 we calculated the intensity of the mobile and immobile species in the red channel. The result of this separation is show in Fig. 4 *B*. As expected, the intensity $\langle F_{M,r}\rangle$ of the mobile dye SR101 (*dashed line*) is time-independent with a value of 48 ± 2 kHz, whereas the intensity of the immobile EGFP $\langle F_{I,r}(t)\rangle$ decays (*solid line*). Next, the fluorescence intensity decay of the red channel (*solid line* of Fig. 4 *A*) was fit to

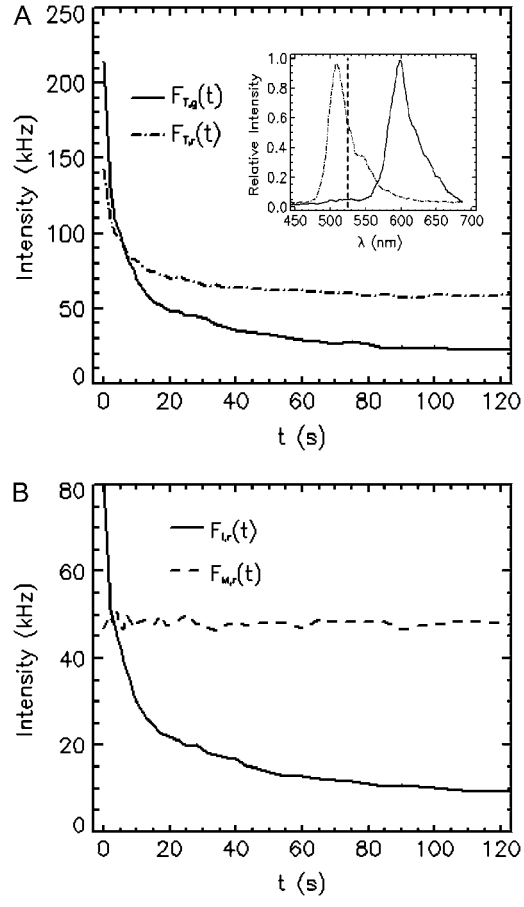

FIGURE 4 Dual-color analysis of immobile EGFP in the presence of the red mobile dye SR101. (*A*) The fluorescence intensity decay of the green channel (*solid line*) and the red channel (*dashed line*). The inset shows the measured emission spectra of EGFP (*dash-dotted line*) and SR101 (*solid line*) together with the transition wavelength of the dichroic mirror (*vertical dashed line*). (*B*) The calculated intensities of EGFP (*solid line*) and SR101 (*dashed line*) in the red channel.

Eq. 29 to determine the intensity of the mobile fraction. The parameters for τ_1, τ_2, and α were constrained during the fit to lie within one standard deviation of the values calibrated previously. The fit to the data shown in Fig. 5 *A* along with the normalized residuals returned a value of 50 ± 3 kHz for the mobile fraction. The values for the intensity of the mobile fraction determined by both methods are identical within experimental uncertainty.

Next we determined the brightness of the mobile species from the fluorescence decay curve. To calculate brightness values, the data of the decay curve are segmented into subsets of approximately constant intensity as described in Materials and Methods. The biased brightness $\lambda^*(t)$ was calculated for each segment according to Eq. 34 with $\gamma_2 = 3/16$ as for a GL PSF and a diffusion time of 0.035 ms, which was determined from the autocorrelation function. As expected, the uncorrected brightness (*solid line*, Fig. 5 *B*) increases with time as the bias introduced by the immobile fraction decreases due to bleaching. The corrected brightness λ is calculated with Eqs. 7 and 8 from the biased value $\lambda^*(t)$ and the intensity $\langle F_{M,r}\rangle$ of the mobile species given above. The corrected brightness is plotted in Fig. 5 *B* (*diamonds*). Its value is time independent with an average of 27 ± 2 kHz (*dashed line*). As a control, the brightness of the dye SR101 was also measured with the same experimental setup in the absence of immobile EGFP, yielding a value of 27 ± 2 kHz. The corrected brightness in the presence of the immobile species is the same as the control value within experimental error.

The procedure of determining the brightness of the diffusing species from the fluorescence decay data was repeated for various concentrations of the mobile dye ranging from ~5 to 500 nM. Fig. 6 *A* shows the corrected brightness values plotted as a function of the initial mobile fraction (*circles*). All of the corrected values lie within 1σ of the expected value of 27 ± 2 kHz (*dashed line*). The uncorrected values $\lambda^*(t=0)$ (*plus signs*) taken at the beginning of each measurement are also shown. The bias decreases as the fractional

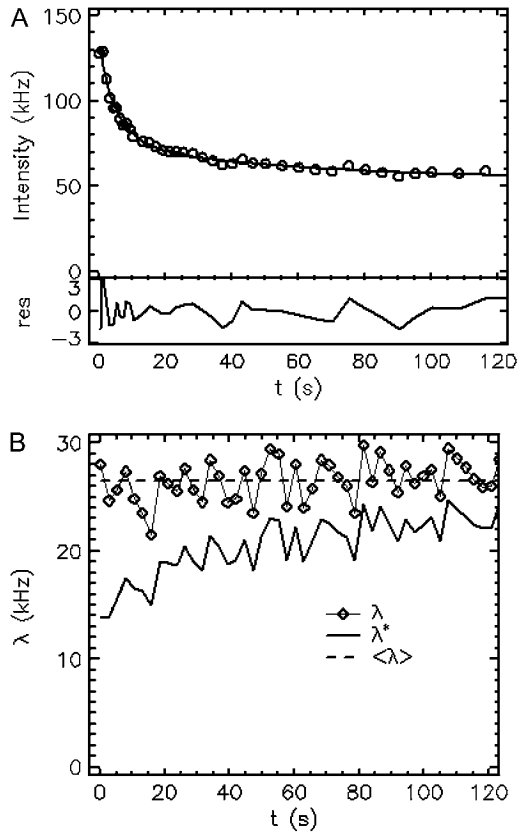

FIGURE 5 (*A*) Intensity decay curve of the red channel is fit to Eq. 31 with the immobile fluorescence modeled by Eqs. 27 and 22. The fit returns an intensity of 50 ± 3 kHz for the mobile dye SR101. The normalized residuals of the fit are shown in the lower panel. (*B*) The uncorrected brightness $\lambda^*(t)$ (*solid line*) and the corrected brightness $\lambda(t)$ (*diamonds*) are shown as a function of time. The average brightness is indicated by the dashed line.

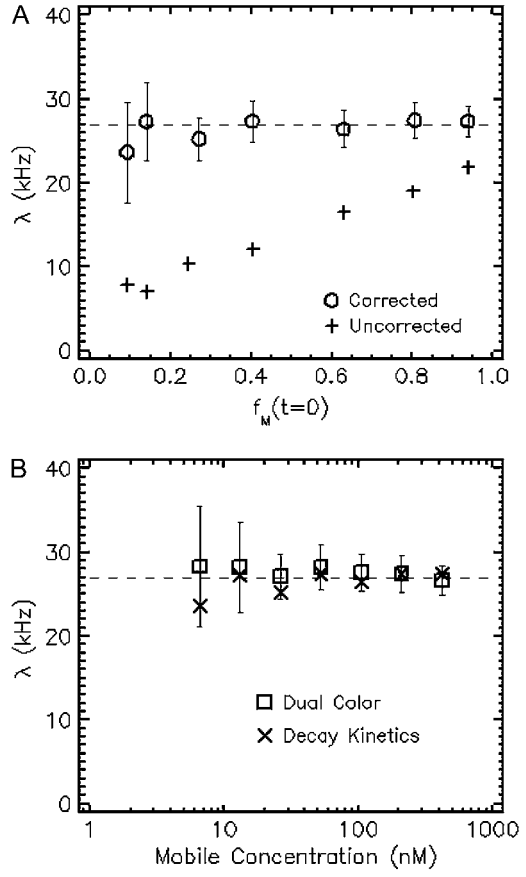

FIGURE 6 Brightness determined for varying amounts of fractional fluorescence intensity f_M of the mobile species. (*A*) The corrected brightness by analysis of the fluorescence decay curve is shown as a function of the initial mobile fraction $f_M(0)$. The uncorrected brightness taken at the beginning of the measurement is also shown. (*B*) Comparison of the corrected brightness determined by the dual-color and the decay kinetics method as a function of the mobile dye concentration. The error bars of the dual-channel data (*squares*) indicate good agreement with the brightness determined by the decay method (*crosses*). The dashed line marks the independently measured brightness of the dye.

intensity of the mobile species increases. Finally, a comparison with the dual-channel method of determining the brightness is shown in Fig. 6 *B* for all measured concentrations. There is good agreement between the two methods across the range of concentrations used in the study. For clarity, the error bars are shown only for the dual-color approach (*squares*).

Measurements inside cells

To demonstrate the applicability of brightness analysis using photobleaching kinetics in living cells, we used the histone core protein H2B as a model system. H2B has been described as having two components: a large immobile fraction incorporated into the chromatin and a small mobile fraction not incorporated (12,13). Because interphase chromatin has a well-regulated structure, we first determined the spatial distribution of H2B in the nucleus by axially scanning the focal point across the cell. Scans across nucleolar locations were excluded. The excitation intensity was chosen to be low enough that photobleaching was negligible during the axial scan. The z-dependent fluorescence intensity of cells expressing H2B-EGFP was recorded. A typical intensity trace is shown in Fig. 7 and displays two intensity peaks. Axial fluorescence scans of the chromatin stained with Hoechst 33342 yielded the same spatial distribution as in the H2B-EGFP case (data not shown). Thus, H2B is not uniformly distributed throughout the nucleus, but appears to localize near the periphery of the cell nucleus. This is consistent with previous findings (13). We modeled the axial H2B-EGFP distribution by assuming that the protein is uniformly distributed at two different heights into independent slabs of some finite thickness. The intensity profile was calculated for this model assuming a GL-PSF. We used a fit algorithm that varies the free parameters until the theoretical intensity profile matches the experimental data. Upon analyzing 10 cells, we found the average thickness of the lower slab to be $z_{th}=$ 3.1 ± 1.1 μm. This value will be used to define the limits in fitting data to the photobleaching model for a slab given by Eq. 25. FFS experiments were performed after the instrument was focused onto the peak position of the fluorescence from the lower slab. The separation between both slabs is large enough that the residual excitation of H2B-EGFP of the upper slab is negligible.

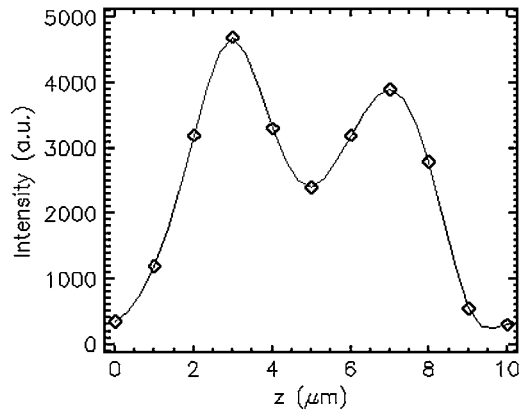

FIGURE 7 Axial intensity trace of a COS-1 cell transfected with H2B-EGFP.

For the initial experiments, cells were cotransfected with H2B-EGFP and monomeric EGFP to ensure that a mobile fraction is present. Five cotransfected cells were measured to determine the mobile fraction and brightness. The parameters for fitting the decay traces were determined from the values given for EGFP measured on the activated cover slides. The measurements in cells were conducted with twice the power used on the activated cover slides. Therefore, the lifetime parameters τ_1 and τ_2 were divided by a factor of 4 to be consistent with the quadratic nature of the two-photon process. The parameter α was unchanged, as it is independent of power. The time-dependent intensity was fit to Eq. 29 to determine the intensity of the mobile component. As discussed above, we used a thickness of 3.1 μm when fitting the intensity decay with Eq. 25. The fluorescence intensity decay is shown together with its fit for one of the measured cells in Fig. 8 *A*. The fit returned an intensity of 81 ± 5 kHz for the mobile species. The biased brightness $\lambda^*(t)$ and the corrected brightness λshown in Fig. 8 *B* were determined in the same manner as for the immobilized slide experiments. The average value for the brightness is 10 ± 1 kHz. The brightness values for all five cells are plotted as a function of the initial mobile fraction $f_M(t = 0)$ in Fig. 9. In addition, the brightness of EGFP was measured independently in the nucleus of cells expressing only the EGFP protein. Its brightness of $\lambda =$ 9 ± 1 kHz serves as a control and is shown in Fig. 9 as an additional data point for a mobile fraction of one. All corrected brightness values are in excellent agreement with this control value.

As stated above, previous experiments have shown that there is a small mobile fraction of H2B moving throughout the nucleus (for a review, see Kimura (26)). More recently, FCS has been used to study the dynamics of this mobility (15). We applied our method on cells transiently transfected with H2B-EGFP. Because we expect a much lower mobile component than in the case of cotransfection with EGFP, these experiments test the applicability of our analysis procedure to cases where the majority of the fluorophores are immobilized. We first calculated the autocorrelation curve of every measured cell. We selected cells with a nonzero correlation amplitude that decays to zero ($\tau_D \sim 2$ ms) for further analysis. For some cells, we observed a correlation trace that decayed much slower (>1 s) and was not described by a simple diffusion process. These cells were discarded from further analysis. The remaining cells were analyzed using the same method as for the cotransfected cells described above. The mobile intensity fraction varied from cell to cell and covered a range from 0.05 to 0.27 as show in Fig. 10. The average brightness value of 8 ± 1 kHz is in good agreement

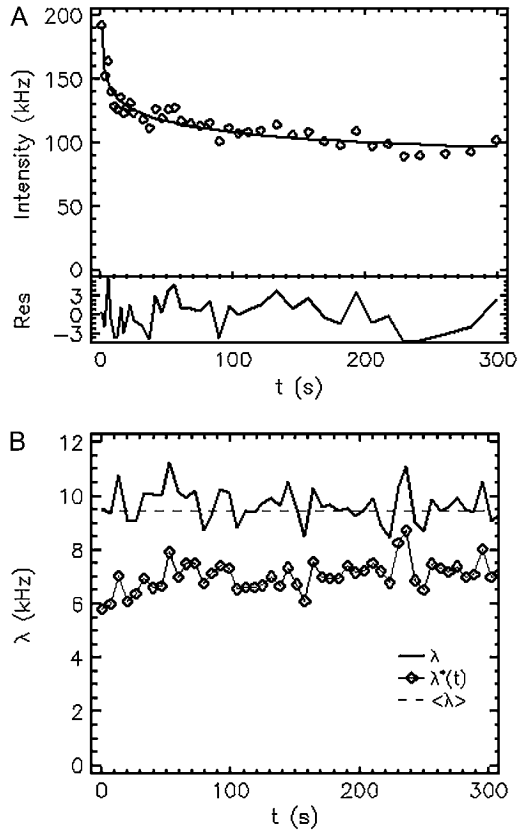

FIGURE 8 Analysis of COS-1 cell cotransfected with EGFP and EGFP-H2B. (*A*) Fit of the fluorescence decay curve to Eq. 31. The intensity of the mobile fluorophores from the fit is 81 ± 5 kHz. The normalized residuals of the fit are shown in the lower panel. (*B*) The uncorrected brightness $\lambda^*(t)$ (*diamonds*) and the corrected brightness $\lambda(t)$ (*solid lines*). The average of the corrected brightness is 9 ± 1 kHz.

with the control brightness measured for EGFP alone. This brightness value is consistent with a model where mobile H2B-EGFP molecules are monomeric when not incorporated in the chromatin.

In the above analysis, the thickness of the slab was fixed to 3.1 μm when fitting the decay curve. Although this value represents the average, the actual thickness for a given cell is not taken into account. To examine the sensitivity of this approximation upon brightness analysis, we performed axial scans to determine the actual slab thickness followed by a kinetic photobleaching measurement of the same cell. The actual thickness was used for determining the brightness from the fluorescence intensity decay curve. These experiments were conducted using a lower power where the calibrated EGFP brightness was determined as 4 ± 1 kHz. The brightness of all measured cells agreed with the calibrated brightness value. In an extreme case, we found a cell with a slab thickness of 4.9 μm. Using this value, the fit to the decay trace from this cell yielded a mobile intensity of 4 ± 2 kHz ($f_M(0) = 0.11$), resulting in a brightness of 4 ± 1 kHz, in good agreement with the expected value. We then used the

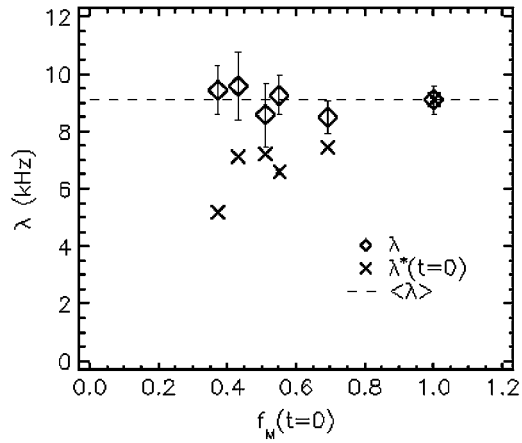

FIGURE 9 Brightness versus mobile fraction of COS-1 cells cotransfected with EGFP and EGFP-H2B. Corrected (*diamonds*) and uncorrected (*crosses*) brightness values are shown as function of f_M. The dashed line shows the calibrated brightness value of monomeric EGFP.

approximation of 3.1 μm, which returned a mobile intensity of 6 ± 1 kHz ($f_M(0) = 0.17$) and a brightness of 3 ± 1 kHz. In this case, the approximation resulted in a lower brightness value than expected for a monomer.

DISCUSSION

We encountered photobleaching of the stationary background fluorescence for all experiments. Although it is possible to lower the laser power sufficiently so that photobleaching is negligible over the timescale of the experiment, it is impractical, because the signal/noise will be insufficient for FFS experiments. Thus it seems that photobleaching of immobile fluorophores is unavoidable. The resulting nonstationary signal requires special attention, because it leads to

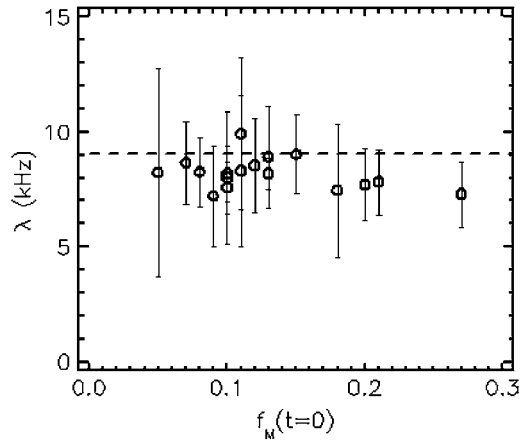

FIGURE 10 Brightness of mobile H2B-EGFP as a function of the initial fraction $f_M(0)$. The brightness of cells transfected with H2B-EGFP was determined by the kinetic photobleaching method. The dashed line at 9 kHz shows the brightness of monomeric EGFP for comparison.

biases in the FFS analysis. To circumvent this problem, we divided the data into segments short enough so that the fluorescence intensity is approximately constant throughout each segment. Although the statistical accuracy decreases for shorter data segments, we have found that it is sufficient to determine the brightness and fluctuation amplitude.

In principle, the problem of a stationary fluorescence source could be avoided by photobleaching the immobile component to zero. As we described earlier, however, the inhomogeneous excitation profile of FFS experiments results in a slow, nonexponential decay of the fluorescence. For example, compare the 2DG and GL model to an exponential decay, where all processes share the same lifetime parameter τ. To photobleach the immobile fluorescence down to 10% requires 2.3τ for the exponential decay, but takes 10τ for the 2DG model and 3000τ for the GL model. Thus, for practical reasons the presence of an immobile species will contribute to the measured signal and must be accounted for.

To account for the bias from the immobile fraction, in a single channel experiment one must adequately describe the kinetics of photobleaching under the given experimental conditions. We found that a sequential two-state process describes the experimentally observed photobleaching kinetics of EGFP, consistent with other studies. We also found that the rate parameters associated with each step vary quadratically with power as expected for a two-photon process. The model presented here assumes that the immobilized EGFP molecules have sufficient rotational mobility, so that polarization effects are negligible. This assumption was tested by comparing photobleaching curves measured with both linear and circular polarized light. We observed no difference in the decay traces (data not shown). Note that it is not necessary to establish the exact physical model of photobleaching for applying the method described in this article. Any parameterization that describes the photobleaching kinetics of the fluorophore under given experimental conditions is sufficient.

Finally, there are limitations to the methods described above. For low fractional intensities f_M of the mobile fluorophores, the accurate determination of its brightness becomes challenging. First, the correction factor needed to calculate the brightness becomes large due to its inverse relationship with f_M. Therefore, any uncertainty in determining f_M leads to large uncertainties in the calculated brightness. In addition, the relative amplitude of fluctuations decreases as the background fluorescence signal increases, which leads to larger experimental uncertainties in calculating FFS parameters. The determination of f_M hinges on extracting the intensity offset $\langle F_M \rangle$ from a fit of the fluorescence decay to Eq. 29. At some point, the mobile fraction will become so small relative to the immobile species that the decay trace can be fit without any offset, which makes the determination of the brightness impossible. The lower limit of f_M for accurate determination of the brightness depends on the experiment. Here we demonstrated that it is possible to extract the brightness of EGFP in cells for a fractional intensity of the mobile protein as low as 5%.

To evaluate the applicability of the kinetic photobleaching technique in cells, we used H2B as a model system. We account for the distribution of the immobilized protein by scanning along the axial direction through the cell. Our data indicate that H2B localizes near the nuclear envelope, consistent with previous studies. Applying a simple slab model resulted in an average thickness of the lower immobilized H2B layer of 3.1 μm, which was used in the subsequent brightness analysis of cells. Because an average value was used, it is important to consider the influence of the thickness parameter on the calculated brightness. Underestimating the real thickness generally results in an increased value of f_M and a reduced brightness, whereas overestimating the real thickness has the opposite effect. Also, for low mobile fractional intensities, fitting of the decay curves is more sensitive to the thickness. The amount of potential bias depends on the specific parameters and has to be evaluated on a case-by-case basis. To minimize the uncertainty in the thickness, it is prudent to directly measure its value on the same cell used for brightness analysis. We demonstrated the feasibility of this approach for cells transfected with H2B-EGFP. Using this method, we recovered the correct brightness in all cases, including a cell with an actual measured thickness of 4.9 μm, where our earlier analysis assuming the average thickness failed.

While the two-slab model describes the H2B system remarkably well, other protein systems most likely require a different model describing the distribution of immobile proteins. The single-slab model is the simplest three-dimensional distribution model. We measured the photobleaching of EGFP in fixed cells and found that using a single slab along the axial axis describes the measured decay trace (data not shown). In general, application of the slab model implies that the immobile fluorophore distribution is approximately uniform across the radial extend of the point spread function. Systems with more complex distributions as described above need to be treated case by case.

Fluorescence recovery after photobleaching and image correlation spectroscopy (ICS) are two other approaches to study and differentiate mobile and immobile molecules (4,27). Improvements of ICS make it possible to filter out the contribution of immobile proteins (28). Because the ICS technique requires images, it is best suited for applications with slow dynamics, such as typically encountered on membranes. Standard FCS, which is based on a point measurement, is more appropriate for systems with fast dynamics, such as proteins diffusing in solution, but does not detect immobilization. This article described a solution for incorporating immobilization into standard FCS experiments. It thus opens up the possibility to quantify fluctuation experiments performed on soluble proteins in the presence of an immobile background, as demonstrated for the H2B system.

Fluctuation spectroscopy is capable of assessing the oligomeric state of a protein by measuring its brightness. For

example, when two monomers form a dimmer, the brightness increases by a factor of 2. In the current model of histone core formation, the free fraction of H2B combines with histone H2A to form the H2A/H2B heterodimer, whereas the histone core of the nucleosome contains two H2A/H2B heterodimers. H2B within the nucleosome is immobilized on the timescale of an FFS experiment as is readily verified by the lack of fluorescence recovery when the excitation light is turned off. Note, in case a significant amount of exchange between immobile and mobile molecules occurs during the duration of the experiment, the theory described in this article has to be modified to account for it. In our analysis, the brightness measured equals that of monomeric EGFP, indicating that only a single copy of H2B-EGFP resides in the mobile protein complex, which is consistent with the H2A/H2B heterodimer model. However, because this study focuses on technique development, experiments are performed with cells that contain endogenous, nonfluorescent H2B that would compete with H2B-EGFP in forming potential multimeric complexes. Biologically relevant applications of the technique need to take the presence of endogenous protein into account.

This article describes a strategy for performing FFS experiments in the presence of immobile fluorophores, and is based on the selective photobleaching of immobile fluorophores. The technique has been tested successfully on EGFP both in vitro and in live cells. Our method should prove useful for the quantitative investigation of proteins interacting with immobile structures in cells, thereby expanding the types of systems for which FFS is applicable.

This work was supported by grants from the National Institutes of Health (GM64589) and the National Science Foundation (PHY-0346782).

REFERENCES

1. Elson, E. L., and D. Madge. 1974. Fluorescence correlation spectroscopy. I. Conceptual basis and theory. *Biopolymers*. 13:1–27.
2. Elson, E. L. 2004. Quick tour of fluorescence correlation spectroscopy from its inception. *J. Biomed. Opt.* 9:857–864.
3. Thompson, N. L., A. M. Lieto, and N. W. Allen. 2002. Recent advances in fluorescence correlation spectroscopy. *Curr. Opin. Struct. Biol.* 12: 634–641.
4. Wiseman, P. W., and N. O. Petersen. 1999. Image correlation spectroscopy. II. Optimization for ultrasensitive detection of preexisting platelet-derived growth factor-beta receptor oligomers on intact cells. *Biophys. J.* 76:963–977.
5. Qian, H., and E. L. Elson. 1990. Distribution of molecular aggregation by analysis of fluctuation moments. *Proc. Natl. Acad. Sci. USA*. 87: 5479–5483.
6. Berland, K. M., P. T. So, Y. Chen, W. W. Mantulin, and E. Gratton. 1996. Scanning two-photon fluctuation correlation spectroscopy: particle counting measurements for detection of molecular aggregation. *Biophys. J.* 71:410–420.
7. Palmer 3rd, A. G., and N. L. Thompson. 1987. Molecular aggregation characterized by high order autocorrelation in fluorescence correlation spectroscopy. *Biophys. J.* 52:257–270.
8. Chen, Y., J. D. Müller, P. T. So, and E. Gratton. 1999. The photon counting histogram in fluorescence fluctuation spectroscopy. *Biophys. J.* 77:553–567.
9. Chen, Y., and J. D. Muller. 2007. Determining the stoichiometry of protein heterocomplexes in living cells with fluorescence fluctuation spectroscopy. *Proc. Natl. Acad. Sci. USA*. 104:3147–3152.
10. Chen, Y., L. N. Wei, and J. D. Muller. 2003. Probing protein oligomerization in living cells with fluorescence fluctuation spectroscopy. *Proc. Natl. Acad. Sci. USA*. 100:15492–15497.
11. Saffarian, S., Y. Li, E. L. Elson, and L. J. Pike. 2007. Oligomerization of the EGF receptor investigated by live cell fluorescence intensity distribution analysis. *Biophys. J.* 93:1021–1031.
12. Lever, M. A., J. P. Th'ng, X. Sun, and M. J. Hendzel. 2000. Rapid exchange of histone H1.1 on chromatin in living human cells. *Nature*. 408:873–876.
13. Kimura, H., and P. R. Cook. 2001. Kinetics of core histones in living human cells: little exchange of H3 and H4 and some rapid exchange of H2B. *J. Cell Biol.* 153:1341–1353.
14. Wachsmuth, M., T. Weidemann, G. Muller, U. W. Hoffmann-Rohrer, T. A. Knoch, W. Waldeck, and J. Langowski. 2003. Analyzing intracellular binding and diffusion with continuous fluorescence photobleaching. *Biophys. J.* 84:3353–3363.
15. Bhattacharya, D., A. Mazumder, S. A. Miriam, and G. V. Shivashankar. 2006. EGFP-tagged core and linker histones diffuse via distinct mechanisms within living cells. *Biophys. J.* 91:2326–2336.
16. Patterson, G. H., S. M. Knobel, W. D. Sharif, S. R. Kain, and D. W. Piston. 1997. Use of the green fluorescent protein and its mutants in quantitative fluorescence microscopy. *Biophys. J.* 73: 2782–2790.
17. Wu, B., and J. D. Muller. 2005. Time-integrated fluorescence cumulant analysis in fluorescence fluctuation spectroscopy. *Biophys. J.* 89:2721–2735.
18. Sanchez-Andres, A., Y. Chen, and J. D. Muller. 2005. Molecular brightness determined from a generalized form of Mandel's *Q*-parameter. *Biophys. J.* 89:3531–3547.
19. Saleh, B. 1978. Photoelectron Statistics. Springer-Verlag, New York.
20. Muller, J. D. 2004. Cumulant analysis in fluorescence fluctuation spectroscopy. *Biophys. J.* 86:3981–3992.
21. Thompson, N. L. 1991. Fluorescence correlation spectroscopy. *In* Topics in Fluorescence Spectroscopy, Vol. 1; 1. J. R. Lakowicz, editor. Plenum, New York. 337–378.
22. Qian, H., and E. L. Elson. 1990. On the analysis of high order moments of fluorescence fluctuations. *Biophys. J.* 57:375–380.
23. Axelrod, D., D. E. Koppel, J. Schlessinger, E. Elson, and W. W. Webb. 1976. Mobility measurement by analysis of fluorescence photobleaching recovery kinetics. *Biophys. J.* 16:1055–1069.
24. Arfken, G. B., and H. Weber. 1995. Mathematical Methods for Physicists. Academic Press, San Diego.
25. Drummond, D. R., N. Carter, and R. A. Cross. 2002. Multiphoton versus confocal high resolution z-sectioning of enhanced green fluorescent microtubules: increased multiphoton photobleaching within the focal plane can be compensated using a Pockels cell and dual widefield detectors. *J. Microsc.* 206:161–169.
26. Kimura, H. 2005. Histone dynamics in living cells revealed by photobleaching. *DNA Repair (Amst.).* 4:939–950.
27. Reits, E. A., and J. J. Neefjes. 2001. From fixed to FRAP: measuring protein mobility and activity in living cells. *Nat. Cell Biol.* 3:E145–E147.
28. Hebert, B., S. Costantino, and P. W. Wiseman. 2005. Spatiotemporal image correlation spectroscopy (STICS) theory, verification, and application to protein velocity mapping in living CHO cells. *Biophys. J.* 88:3601–3614.